Bidirectional fear modulation by discrete anterior insular circuits in mice

Sanggeon Park[1,2†], Yeowool Huh[3,4†], Jeansok J. Kim[5*], and Jeiwon Cho[1,2*]

[1] Department of Brain and Cognitive Sciences, Scranton College, Ewha Womans University, Seoul, Republic of Korea

[2] Brain Disease Research Institute, Ewha Brain Institute, Ewha Womans University, Seoul, Republic of Korea

[3]Department of Basic Medical Science, College of Medicine, Catholic Kwandong University, Gangneung, Gangwon-do, Republic of Korea

[4]Institute for Bio-Medical Convergence, International St. Mary's Hospital, Catholic Kwandong University, Incheon, Republic of Korea

[5]Department of Psychology, University of Washington, Seattle, WA, USA

† Co-first authors: Sanggeon Park and Yeowool Huh equally contributed to the study.

*Correspondence and requests for materials should be addressed to: J.C. and J.J.K. (jelectro21@ewha.ac.kr and jeansokk@uw.edu)

ABSTRACT

The brain's ability to appraise threats and execute appropriate defensive responses is essential for survival in a dynamic environment. Humans studies have implicated the anterior insular cortex (aIC) in subjective fear regulation and its abnormal activity in fear/anxiety disorders. However, the complex aIC connectivity patterns involved in regulating fear remain under investigated. To address this, we recorded single units in the aIC of freely moving mice that had previously undergone auditory fear conditioning, assessed the effect of optogenetically activating specific aIC output structures in fear, and examined the organization of aIC neurons projecting to the specific structures with retrograde tracing. Single-unit recordings revealed that a balanced number of aIC pyramidal neurons' activity either positively or negatively correlated with a conditioned tone-induced freezing (fear) response. Optogenetic manipulations of aIC pyramidal neuronal activity during conditioned tone presentation altered the expression of conditioned freezing. Neural tracing showed that non-overlapping populations of aIC neurons project to the amygdala or the medial thalamus, and the pathway bidirectionally modulated conditioned fear. Specifically, optogenetic stimulation of the aIC-amygdala pathway increased conditioned freezing, while optogenetic stimulation of the aIC-medial thalamus pathway decreased it. Our findings suggest that the balance of positive and negative neuronal activity in the aIC and the distinct efferent circuits interact collectively to modulate fear behavior.

INTRODUCTION

Pavlovian fear conditioning is believed to serve a survival function in nature and is widely used as a preclinical model system to understand normal and abnormal fear behavior in humans (1-3). Functional brain imaging studies consistently implicate the insular cortex (IC) in processing fear and anxiety in humans. Specifically, healthy subjects show increased IC activity with fear conditioning (4-9), while patients with anxiety disorders exhibit even greater IC activity (10-12). Animal studies also implicate the IC in fear conditioning. For instance, re-exposure of rodents to a fear-conditioned context increases IC activity as measured by c-Fos or cytochrome oxidase staining (13, 14). Additionally, microinjection of cobalt chloride, a non-selective synapse blocker, in the IC disrupts fear conditioning (15), and post-training electrolytic lesions of the IC attenuate the expression of conditioned fear (16).

Anatomically, the IC is divided into the anterior IC (aIC) and posterior IC (pIC) by the middle cerebral artery. Although they are reciprocally connected, the aIC and pIC have distinct connections with other brain regions (17-19). Specifically, the pIC receives inputs from the primary somatosensory thalamic nuclei, while the aIC receives strong inputs from the prefrontal cortex and has reciprocal connections with higher-order association thalamic nuclei, such as the mediodorsal thalamus. Given its connections with cortical brain regions, the aIC is ideally positioned to integrate high-level information to regulate behaviors. Although both aIC and pIC have been implicated in fear conditioning (15, 20-23), how the aIC connections to different brain regions modulate fear remains unclear.

Therefore, in this study, we investigated how the aIC neurons projecting to different brain regions process auditory fear conditioning. Using single-unit recording, we found that a subset of aIC pyramidal neurons displayed activity that was positively or negatively correlated with a conditioned freezing response, suggesting that the balance of different aIC neuronal activities regulates fear behavior. Neural tracing revealed that distinct population of

aIC neurons projects to the amygdala and the medial thalamus. Optogenetic manipulations confirmed that the aIC exerts bidirectional modulation of fear behavior through the aIC-amygdala pathway (increases fear) and the aIC-medial thalamus pathway (decreases fear). Together, our study suggests that different aIC circuits are involved in bidirectional modulation of fear behavior.

Results

aIC activities correlate with conditioned fear

To investigate how conditioned fear is processed by individual aIC neurons, we recorded their activity during the expression of auditory fear (conditioned group) or to tone presentation (control group) (Figure 1A). We histologically verified the recording locations to be within the aIC including the dorsal agranular insular cortex (AID), ventral agranular insular cortex (AIV), dysgranular insular cortex (DI), and granular insular cortex (GI) (Figure 1B). Most unit signals were recorded from the AID and AIV. We only used well-isolated unit signals from the aIC for analysis (Figure 1C). Of the recorded neurons, we analyzed the activity of 108 putative pyramidal neurons from 11 mice, which were distinguished from putative interneurons (n = 8 cells) based on the characteristics of their recorded action potentials (Figure 1D; see methods for details).

As expected, the auditory fear conditioned mice significantly increased their freezing behavior during the tone conditioned stimulus (CS) presentation (Figure 1E, repeated-measures ANOVA, $F_{(35,210)} = 11.303$, $P < 0.001$), particularly during tone-on periods compared to tone-off periods (Figure 1F left, paired samples t-test, $P < 0.001$). In contrast, control mice that did not undergo auditory fear conditioning showed virtually no freezing

during the tone presentation (Figure 1E, F).

The mean of all normalized (z-scored) pyramidal neuronal activities recorded in the aIC remained steady during the experiment in both groups (Figure 1G). The conditioned group showed no significant correlation between the normalized firing rate and freezing behavior, nor was there any difference in the mean firing rate between the tone-on and tone-off periods (Figure 1H). Similar trends were observed in the normalized neuronal activity of control mice (Figure 1G, H). These results suggest that the mean activity of all recorded aIC pyramidal neurons remains relatively constant, regardless of the fear experience.

Several studies report reduction in theta frequency in presence of the CS in several brain regions including the hippocampus, medial prefrontal cortex, and amygdala (24-26). Similarly, the power of aIC local field potential in the <50 Hz frequency, which includes the theta frequency, tended to be reduced in the conditioned group compared to the control during CS (Figure 1I, J). Quantitative analysis revealed that theta frequency (6 Hz) was significantly reduced during, but not before, CS presentation in the conditioned group compared to the control (Figure 1K).

To examine the relationship between firing rates of individual neurons and conditioned freezing behavior in detail, we attempted to identify a population of neurons whose activity changed in response to the conditioned tone stimulus. Using Pearson's correlation analysis, we identified three types of aIC neuronal responses: neurons whose firing rate increased in parallel with the freezing response ("positive cells"), neurons whose firing rate decreased with freezing ("negative cells"), and neurons that had no significant changes correlated with freezing ("non-responsive cells"). The distribution of all coefficients is shown in Figure 2A. Among the neurons recorded from fear conditioned mice, 29.6% were responsive (n = 32/108) and 70.4% were non-responsive (n = 76/108) (Figure 2A). Among the responsive cells, there were proportionally more positive cells (n = 21/32, 65.6%) than negative cells (n = 11/32,

34.4%), but the trend was not statistically significant (binomial proportions test, $P = 0.11$) (Figure 2A).

Histological analysis of the recording locations of respective neuronal-response types suggested that the positive and negative cells may be located in different layers of the aIC (Figure 2B). The positive cells tended to be recorded in the middle and deep layers (L5 and 6; Figure 2B, red dots), while the negative cells tended to be recorded in the superficial and middle layers (L2/3, 4, and 5; Figure 2B, blue dots). Tetrodes that recorded both positive and negative cells tended to be located in the middle layer (L5; Figure 2B, red and blue gradation dot). The non-responsive cells were recorded from all layers of the aIC. To visualize any differences in firing rate changes among different neuronal-response types in fear conditioned and control mice, the mean normalized firing rate of individual aIC neurons was sorted in ascending order of their respective Pearson's correlation coefficients (Figure 2C). Negative cells showed relatively higher tone-off firing rates, which decreased during tone presentation (Figure 2C, conditioned upper). Positive cells, in contrast, showed a lower tone-off firing rate that increased during tone presentation (Figure 2C, conditioned lower). The non-responsive cells, interestingly, showed an intermediate tone-off firing rate between those of the negative and positive cells and remained relatively constant throughout the recording (Figure 2C, conditioned middle). The neuronal activity of control mice was similar to the non-responsive cells of the fear conditioned mice (Figure 2C, control). Sample raster plots during the five CS presentations and peri-stimulus time histogram (PSTH) of a negative and a positive cell consistently show the trend (Figure 2D). The differences in baseline firing rate of different cell-response types are also reflected in raw, not normalized, values (Figure 2E; one-way ANOVA, $F=6.65$, $P<0.001$). These results suggest that subpopulations of pyramidal neurons in the aIC may become primed to respond to the fear-conditioned stimulus.

To visually present the relationship between aIC neuron's response type and conditioned

fear expression, we plotted normalized neuronal activities of each neuronal response type and freezing behavior over the time course of the fear expression test. Analysis revealed a tight relationship between the activity of positive and negative cells and freezing behavior (Figure 2F, G). The mean activity of positive cells mirrored freezing behaviors, increasing activity at peak freezing (Figure 2F), whereas the mean activity of negative cells decreased during freezing behavior (Figure 2G). Non-responsive cells showed no apparent changes that were correlated with freezing responses (Figure 2H). Pearson's correlation coefficient between mean normalized firing rate and freezing revealed that the activities of the positive and negative neurons were significantly correlated with freezing behavior in opposite directions (positive cell r = 0.81, $P < 0.05$; negative cell r = -0.68, $P < 0.05$). As expected, no correlation was found for the non-responsive neurons (r = 0.13, $P = 0.44$). For detailed analysis of each neuronal response type's activity changes that occurs during CS, we compared the absolute values of negative and positive cells in smaller time bins (1 s). The tone-induced firing rate peaks of the negative and positive cells were significantly different (Figure 2I, Mann-Whitney Test, $P < 0.05$); the negative cells peaked at 10.5 s, while the positive cells peaked at 17.6 s. This difference suggests differential circuits may regulate the activities of different neuron types in response to fear.We also analyzed additional qualities of the aIC neurons, such as the presence of neurons that precisely signaled the beginning or termination of the tone, the tone on-set and tone off-set cells, respectively. However, none of the recorded aIC neurons, neither the conditioned group's nor the control's, were tone on-set or tone off-set cells.

We then assessed the correlation between neuronal activity and tone. None of the neuronal activity of control mice (n = 13 cells, 3 mice) significantly correlated with the tone (r = 0.027, $P = 0.87$), but a subset of aIC neurons in conditioned mice showed significant correlation with tone (positive cells, r=0.44, $P<0.05$, n=9; negative cells, r=-0.51, $P<0.05$,

n=5). During the five-tone presentation, however, freezing behavior was still high, and therefore difficult to distinguish whether aIC neuronal activities correlate with freezing, tone, or both. To differentiate what the aIC neuronal activities represents, we carried out a fear extinction experiment (Figure 2J) where conditioned freezing behavior reduces gradually over the ten trials (Figure 2K). Just like the five-tone presentation experiment, we found the positive and negative cells that correlated with freezing (Figure 2L). Pearson's correlation coefficient between mean normalized firing rate and freezing show that the activities of the positive and negative cells were significantly correlated with freezing behavior in opposite directions (Figure 2M; positive cells, $r = 0.81$, $P < 0.05$; negative cells, $r = -0.68$, $P < 0.05$). Interestingly, none of the recorded cells correlated with tone (Figure 2N). Together, these results suggest that the positive and negative cells found in the aIC of fear-conditioned mice are highly correlated with freezing behavior, not tone.

Manipulating aIC activities modulate conditioned fear behavior

Our results suggest that the emergence of positive and negative cells following fear conditioning may be critical in regulating freezing (fear) behavior. To investigate this further, we tested whether artificially increasing or decreasing the activity of aIC pyramidal neurons with optogenetics could affect freezing behavior. Viral vectors were used to express channelrhodopsin-2 (ChR2: AAV-CaMKII-ChR2-eYFP), halorhodopsin (NpHR3: AAV-CaMKII-NpHR3-eYFP), or fluorophore (control: AAV-CaMKII-eYFP) in the aIC pyramidal neurons and we assessed how optical stimulation affects conditioned fear behavior in each group (Figure 3A). We only analyzed the behavior of mice with confirmed viral expression in the aIC (Figure 3B). In a separate group of mice, we assessed whether optical stimulation induces aberrant behaviors or affects locomotion with the open field test. Neither activation of ChR2 nor NpHR3 triggered any aberrant behaviors, and locomotion did not differ among

groups (Figure 3C). Optical stimulation of ChR2 or NpHR3 specially activated or inhibited the activity of aIC pyramidal neurons. respectively (Figure 3D, E). ChR2 stimulation increased brain rhythms in the 20 Hz and 40 Hz range (Figure 3D, spectrogram) because light stimulation was delivered at 20 Hz pulses. Continuous light was delivered for NpHR3 stimulation, so it did not induce specific frequency modulation (Figure 3E, spectrogram). Simultaneous local field potential (LFP) and single unit analysis before, during, and after optical stimulations confirmed that optostimulation of the aIC neurons did not induce aberrant seizure-like synchronized activities.

After confirming that optical activation parameters used in the study does not interfere with locomotion, we examined whether optogenetically manipulating the activity of aIC pyramidal neurons modulates conditioned freezing behavior. As predicted, optogenetic excitation or inhibition of aIC pyramidal neurons in the right hemisphere produced distinct changes in freezing behavior (Figure 3F). During a 30 s tone+optostimulation, there was no difference in freezing behavior among groups (Figure 3G; Kruskal-Wallis, $H(2) = 2.489$, $P = 0.288$). However, during the tone-off sessions, freezing behavior among groups differed significantly (Figure 3G; Kruskal-Wallis, $H(2) = 22.937$, $P = 0.000$; post hoc Mann-Whitney, ChR2 vs. control $P = 0.000$; NpHR vs. control $P = 0.019$). Conditioned freezing responses of the ChR2 group were sustained even after tone+optostimulation ended, and tended to accumulate with repeated stimulations, particularly during the tone-off sessions. This was distinct from the conditioned freezing responses observed in the NpHR3 or control groups (Figure 3G). In the NpHR3 group, freezing immediately decreased after tone+optostimulation ended (Figure 3G). When comparing the freezing behavior of each group during their first and last tone+optostimulation trials, inhibition of aIC pyramidal neurons (NpHR3) reduced the freezing level between the first and the last tone+optostimulation (Figure 3H, left; Wilcoxon signed test, $P = 0.063$). During the tone-off

period, the ChR2 group significantly increased freezing after the last stimulation compared to the first (Figure 3H, right; Wilcoxon signed test, $^{**}P < 0.01$).

These group differences in fear expression were absent in the experiment carried out without optostimulation (ANOVA group effect: $F_{(2,30)} = 1.076$, $P = 0.354$) (Figure 3I, J), confirming that group differences in fear expression were induced by the activation or inhibition of pyramidal neurons in the aIC. Likewise, the accumulative influence in behavior was absent without optostimulation (Figure 3K).

Distinct aIC circuits bilaterally control conditioned fear

Despite optogenetic modulation of aIC pyramidal neurons affecting fear behavior, the effect was unclear, as there were no differences in freezing behavior during optical stimulation delivery among groups. One possible explanation for this is that the aIC circuits that regulate fear behavior in opposing directions were simultaneously activated to cancel out the effects. To investigate further, we looked into aIC projections to various brain areas that could potentially influence fear behavior. The aIC projects to the amygdala (BLA, basolateral amygdala; and CeA, central amygdala) and the medial thalamus (MD, mediodorsal thalamus; and CM, centromedial thalamus) (19). Of the many brain regions the aIC project to, we focused on these brain areas due to their known involvement in fear regulation and the lack of reciprocal connections between them and the pIC.

To investigate whether the same or different population of neurons in the aIC project to the medial thalamus and the amygdala using retrograde tracer injections (Figure 4A). Two different colors of fluorophore-conjugated Cholera toxin subunit B were injected into the medial dorsal thalamus (Alexa Fluor 594, red) and the amygdala (Alexa Fluor 488, green) in each mouse (Figure 4B, C). A week later, fluorophore expression was examined in the aIC region. Surprisingly, none of the neurons in the aIC expressed both green and red

fluorophores, suggesting that non-overlapping populations of aIC neurons project to the medial dorsal thalamus and the amygdala (Figure 4D). The neurons projecting to the medial dorsal thalamus and the amygdala were also located in different layers within the aIC; the aIC neurons projecting to the medial dorsal thalamus appeared mainly in the deep layers (approximately layer 6), while the aIC neurons projecting to the amygdala appeared in a relatively more superficial layer (approximately layer 5). Few aIC→amygdala neurons were present in layer 6, but we found no aIC→medial thalamus neurons in layer 5. The number of aIC neurons projecting to the medial dorsal thalamus was greater than those projecting to the amygdala even though they were populated in a more restricted area (Figure 4E). Although the recording location of the positive and negative cells does not exactly match the tracing results, positive cells were recorded from deep layers while negative cells were recorded from middle and superficial layers (Figure 2B). Collectively, data suggest that the aIC→medial thalamus neurons could be positive cells, while the aIC→amygdala neurons may be negative cells.

To distinguish the roles of the aIC→medial thalamus and the aIC→amygdala projections, we performed bilateral optical stimulation of the respective aIC terminals expressing ChR2 during the expression of conditioned fear (Figure 5A, E). As shown in the sample expression patterns, the aIC projection toward the thalamus terminated mainly in the MD and CM regions (Figure 5B), while the aIC projection toward the amygdala terminated mainly in the BLA and CeA (Figure 5F). Interestingly, activation of the aIC→medial thalamus and the aIC→amygdala projections induced completely different effects. While activating the aIC→medial thalamus projection significantly reduced freezing compared to the control (Figure 5C, blue line; repeated measures ANOVA, $F(1, 17) = 10.666$, *** $P < 0.001$), activating the aIC→amygdala projection significantly enhanced freezing compared to the control (Figure 5G, red line; repeated measures ANOVA, $F(1, 12) = 23.663$, *** $P < 0.001$).

Also, when opto-stimulation was turned off, and only the conditioned tone was delivered (retrieval test), there were no differences in the freezing level between groups (Figure 5C, G). The results indicate that the behavioral differences were indeed induced by the activation of respective projections. In addition, we compared freezing levels of tone+optostim and tone-off periods to assess whether activation of these pathways produces a lasting effect on behavior. Unlike the phenomenon observed in aIC activation with ChR2 (Figure 3F), activation of neither the aIC→medial thalamus nor the aIC→amygdala projection produced any lasting behavioral effects between light stimulations (Figure 5D, H). The tracing and optogenetics manipulation results support the hypothesis that distinct hardwired circuits of the aIC, one projecting to the amygdala and the others projecting to the medial thalamus, regulate conditioned fear bidirectionally.

Discussion

Our study shows that neuronal activity in the aIC can regulate conditioned fear behavior bidirectionally via at least two different subpopulations of neurons that project either to the amygdala or the thalamus. Specifically, we found two types of aIC pyramidal neurons whose activity positively or negatively correlates with conditioned fear behavior, consistent with our previous finding that restraint stress-induced defensive behaviors (23) correlate with the activity of aIC pyramidal neurons. While previous studies have reported positive or negative responses to conditioned stimuli in different conditioning paradigms and brain areas, including the pIC (27), our study found that the ratio of these neurons differed in the aIC. In the pIC, a significantly larger population of positive neurons was reported compared to negative neurons (27), but in the aIC, we found approximately an equal number of positive and negative neurons. The brain's balance between excitation and inhibition (E/I) has been

proposed to play a crucial role in its normal functioning. An E/I imbalance has been linked to various disorders, such as epilepsy, schizophrenia, and autism spectrum disorder (28). Our study's finding of an approximately equal number of positive and negative cells in the aIC, compared to the pIC, suggests that the aIC may be more specialized in maintaining the E/I balance, possibly by activating different circuits.

While both the positive and negative aIC cells showed significant correlations with freezing behavior, their temporal firing rate changes during CS presentation were different. Specifically, the activity of the negative cells dropped before the positive cells increased in response to the CS presentation. Previous studies have demonstrated that temporal differences in the arrival of excitatory and inhibitory inputs can create a time window for local signals to be transmitted while maintaining the global E/I balance (29, 30). We hypothesize that the observed differences in the temporal activity of the positive and negative aIC cells may provide such a window for orchestrating signal gating and processing. This suggests that the aIC may play a critical role in regulating the balance between excitation and inhibition during fear conditioning.

Although this study was unable to determine what determines an aIC neuron to be a positive or negative response type, we speculate that inputs from different brain areas may influence the different responses. For instance, negative cells may receive input from the prefrontal cortex since whole-brain connectivity analysis of the IC indicated that the prefrontal cortex provides more inputs to inhibitory neurons in the aIC than to excitatory neurons(19). Conversely, positive cells may receive input from the amygdala, as the amygdala provides more input to excitatory neurons in the aIC than inhibitory neurons (19).

Given the potential importance of positive and negative neurons in conditioned fear processing, we investigated whether disrupting the E/I balance by optogenetically increasing or decreasing the total output of aIC pyramidal neurons could alter fear behavior (freezing).

Our findings demonstrated that fear behavior could be bidirectionally modulated by aIC neuronal activity: exciting aIC neurons increased the fear response, while inhibiting aIC neurons had the opposite effect. These findings have significant clinical implications since they suggest that specifically targeting negative or positive cells for neuromodulation may not be necessary to have a therapeutic effect. Even though the aIC has fine microcircuitry and intricate connections with many brain regions, merely controlling the total output of the aIC may be enough to regulate fear and anxiety disorders.

During the aIC optogenetic stimulation, we observed a phenomenon where brief excitation or inhibition of aIC pyramidal neurons had a residual effect on behavior during the inter-trial period when optic stimulation was off. Another study also reports the cumulative effects of optical activation of ChR2-expressing neurons on freezing behavior even after optic stimulation ended (31), supporting that it can happen. Although further studies will be necessary to verify what causes this phenomenon, our single unit recording and local field potential analysis during optostimulation support that it is not due to seizure produced by optostimulations. It may occur due to the recruitment of several brain areas modulated by the aIC neurons since activating a more specific circuit, the aIC→medial thalamus or the aIC→amygdala projection, did not produce any lasting effects between light stimulations. Activation or inhibition of the aIC may promote or reduce activation of a recurrent circuit that controls behavior, especially since the aIC has connections with motor-related brain regions (19).

In addition to our finding that optically controlling the total output of the aIC bidirectionally and cumulatively regulates fear behavior, we found that selective activation of distinct non-overlapping population of aIC neurons projecting to different brain regions produced clear-cut bidirectional changes in fear behavior. Specifically, optical activation of the aIC projection to the amygdala enhanced and sustained fear behavior, while activation of

the aIC projection to the thalamus reduced fear behavior. Our results are consistent with previous studies reporting that amygdala activation promotes fear responses (32), while thalamus activation, especially in the burst firing mode of the MD, reduces fear responses (33, 34). Although terminal optogenetic stimulation could produce antidromic activation (35), it only activates a subset of aIC neurons projecting to the areas, Therefore, our study demonstrates for the first time that controlling distinct aIC outputs bidirectionally regulate fear behaviors.

Although we do not have a direct link between single-unit recording and aIC projections, the recording locations of the positive and negative cells suggest that medial thalamus projecting neurons could be positive cells while the amygdala projecting neurons may be negative cells. If so, then the activity of the aIC neurons would work as a mechanism to reduce overexpression of fear. Similar to our findings, the insular→central amygdala and the insula→nucleus accumbens differentially regulated fear (36). Since the insular cortex is extensively connected with various brain regions (19), several redundant circuits may be present in the aIC to fine-tune fear behavior. How the fear promoting and fear reducing aIC circuits compete and cooperate is still unclear and it would be interesting to investigate this in future studies.

In conclusion, our study provides evidence that the aIC regulates conditioned fear behaviors through bidirectional control on multiple levels, with the balance of positive and negative neuronal activity operating at the local circuit level and different populations of neurons projecting to different brain regions exerting additional control. These findings contribute to our understanding of the neural circuits underlying fear behavior and have potential implications for the development of novel therapeutic strategies for fear and anxiety disorders.

Methods

Animals

All experiments were conducted in accordance with the guidelines of the Institutional Animal Care and Use Committee (IACUC) of Ewha Womans University (EWHA IACUC 21-008-t), and all efforts were made to minimize animal suffering. Our research is in accordance with ARRIVE 2.0 guidelines (37). We used F1 hybrids of C57BL/6J × 129/SvJae male mice (10-18 weeks old) in our experiments. The mice were housed at a constant temperature (23 ± 1 °C) and humidity level (50 ± 5%). They were kept in home cages with free access to food and water and subjected to an alternating 12-hour dark-light reversal cycle starting at 9 am. Following the microdrive or optic ferrule implantation, the initially group-housed mice were individually caged.

Auditory fear conditioning

All mice were handled for at least one week before the experiments. For conditioning, we used a fear conditioning chamber (Coulbourn Instruments, Allentown, PA) equipped with stainless-steel bars on the floor for delivering electric foot shocks, placed inside an isolation box with a camera mounted on its ceiling. A day before conditioning, the mice were habituated in a white acrylic cylinder (context A: diameter * height = 20 * 25 cm) for 10 min. Twenty-four hours after habituation, the mice were exposed to three conditioning tones (CS; 2 kHz, 75 dB) lasting 30 s, which were co-terminated with a foot shock (US: 0.5 mA, 1 s) at 2.5-min inter-trial intervals in the fear conditioning chamber (context B; width * length * height = 18 * 18 * 29 cm). The expression of conditioned fear was tested the following day in context A. The freezing response was defined as the absence of any movement (other than breathing) for >1 sec and was videotaped and manually scored by two investigators who were

blinded to the experimental groups.

Surgery for single unit recording

Mice were anesthetized with Zoletil (30 mg/kg, i.p.) and then fixed to a stereotaxic instrument (David Kopf Instruments, USA) for surgical procedures. After craniotomy, a microdrive was implanted into the anterior insular cortex (AP: +1.2 mm, ML: -3.4 mm, DV: -1.8 mm, mouse brain atlas (38)) for behavioral single-unit recordings. The microdrive was equipped with four tetrodes, where 12.5 μm Nichrome polyamide-insulated microwires were intertwined into one tetrode, Kanthal precision technology. The recording tip of each tetrode channel was gold-plated to have a resistance of 300 – 400 kΩ measured at 1 kHz (Bak Electronics, USA). After implantation, the microdrive was secured onto the skull with self-tapping stainless-steel screws and dental cement (Vertex Dental, Netherlands). Mice were allowed to recover from surgery for at least one week before experiments.

Single unit recording and expression of conditioned auditory fear

We used a behavioral single-unit recording technique to investigate the activities of individual neurons during exposure to the CS (tone) after auditory fear conditioning. Screening for neuronal activity was carried out in a square black chamber (width * length * height = 20 * 23 * 14 cm). To obtain unit signals, neural signals were amplified (x10,000), filtered (600 Hz to 6 kHz), and digitized (30.3 kHz) using Digital Lynx (Neuralynx, Tucson, AZ). Upon successful identification of unit signals, mice underwent habituation in context A, followed by the auditory fear conditioning process in context B the next day. No neuronal activities were recorded during this period. The day after conditioning, single neurons were recorded in freely behaving mice during the expression of auditory fear in context A. Neuronal activity and videos were recorded simultaneously and synchronized by the

Neuralynx data acquisition system. Tone (CS; 2 kHz, 75 dB, lasting 30 s) event times were saved using Transistor-Transistor Logic (TTL) signals. The baseline was recorded for 3 min, and then behavior and neuronal activities during five CS (30 s), each separated by a 2.5-min inter-trial interval, were recorded. Neuronal signals were manually isolated into single units using Spike Sort 3D (Neuralynx, USA). The quality of isolated unit signals was assessed by L-ratio, isolation distance, inter-spike intervals in the ISI histogram (ISI > 1 ms) provided by the software, and cross-correlation analysis. We only used well-isolated units that were confirmed to be recorded in the aIC (conditioned group: n = 116 neurons, 11 mice; control group: n = 14 neurons, 3 mice) for the analysis. The mean of units used in our analysis are as follows: L-ratio = 0.09 ± 0.012, isolation distance = 44.97 ± 5.26 (expressed as mean ± standard deviation).

Single unit recording analysis

Isolated single-unit signals were separated into putative pyramidal neurons (conditioned group: *n* = 108 neurons, 11 mice; control group: *n* = 13 neurons, 3 mice) or putative interneurons (conditioned group: *n* = 8 neurons, 7 mice; control group: *n* = 1 neuron, 1 mouse) using action potential duration and repolarization time (23). We only used data from putative pyramidal neurons in our analysis. Firing rates of putative pyramidal neurons were normalized using the z-scored method: *value*=firing rate at a given time bin, μ=mean firing rate of the total recording session, σ=standard deviation of the total recording session. The time bin size of neuronal signal analysis was 30 s.

$$z = \frac{value - \mu}{\sigma}$$

The relationship between neuronal activity and behavior was analyzed by calculating Pearson's correlation coefficient between normalized firing rate (z-score) and freezing behavior. Based on the significance of Pearson’s correlation coefficient (p-values < 0.05),

neurons were classified as positive-response cells (significant positive correlation), negative-response cells (significant negative correlation), or non-responsive cells (no significant correlation).

Local field potential analysis

Local field potential (LFP) was simultaneously obtained with single unit recording. LFP frequency (1–120 Hz) changes induced by tone was analyzed with the *mtspecgramc* function from the Chronux toolbox (39) . Normalized (z-scored) LFP power of the five tones before (20 s), during (30 s), and after (20 s) CS presentation were used to plot the spectrogram of the conditioned and control groups. To compare LFP power at different frequencies in presence and absence of tone in each group, a power spectrum was plotted with the Chronux toolbox's *mtspectrumc* function. Since previous studies report changes in theta power with fear conditioning in other brain regions (24-26), we analyzed the difference in theta (6 Hz) between groups in presence and absence of tone.

Surgery for optogenetic studies

For the optogenetic studies, general anesthesia was induced in mice with 2.5% isoflurane (room air as the carrier gas) and maintained at 1.0% (Somnosuite, Kent Scientific) throughout surgical procedures. A 33-gauge blunt needle attached to a Nanofil (WPI, USA) was used for viral injections (500-600 nL/brain site). The injection speed was set at 100 nL/min, and injection needles were placed in the target site for 10 min before and after viral injection. Viruses with an alpha-calcium/calmodulin-dependent protein kinase II (CaMKIIα) promoter, which targets pyramidal neurons, were injected into the aIC (AP: +1.2 mm, ML: -3.4 mm, DV: -1.8 mm) for optogenetic control of excitatory pyramidal neurons. The types of viruses used for the study were AAV2-CaMKIIα-ChR2-EYFP (n=13), AAV2-CaMKIIα-eNpHR3.0-

EYFP (n=7), and AAV2-CaMKIIα-EYFP (n=13) (UNC Vector Core, USA). An optic fiber (multimode 62.5-μm core optic fiber) attached to a ceramic ferrule (Thorlabs, USA) was implanted unilaterally into the right aIC (AP: +1.2 mm, ML: -3.4 mm, DV: -1.75 mm). For stimulation of the aIC-amygdala or the aIC-medial thalamus projections, optic fibers were bilaterally implanted in the amygdala (AP: -1.2 mm, ML: ±3.4 mm, DV: -4.25 mm) or the medial thalamus (AP: -1.2 mm, ML: ±1.21 mm, DV: -2.53 mm, angle: ±15°). Optic ferrules were secured onto the skull with self-tapping stainless-steel screws and dental cement (Vertex Dental, Netherlands). Mice for optogenetic experiments were allowed to recover for at least 2 weeks to allow sufficient time for viral expression.

Open field test with optogenetic stimulation

To assess whether optostimulation parameters used in our study may influence behavior and interfere with the interpretation of the results, we analyzed the behaviors of mice in the three groups (ChR2, NpHR3, control) with optostimulation recorded in an open field. Mice were released in an open field chamber (50×50×50 cm opaque white acrylic, ~75 lx) and allowed to explore for 3 min (baseline). Then, five 30-s optostimulations (light on) were delivered with an interval of 30 s (light off). The same optostimulation parameters used for the fear test was applied (ChR2: 20 Hz, 473 nm, 3-8 mW; NpHR3: continuous, 593 nm, 6-8 mW; control: 20 Hz, 473 nm, 3-8 mW). We used the Ethovision software to analyze the velocity (cm/s) of the three groups during baseline, light on, and light off.

Neuronal recording with optogenetic stimulation

Changes in single unit activities and brain rhythms (LFP) induced by optostimulation were measured using a custom made optotetrode (microdrive with an optic fiber and 4 tetrodes, Axona, UK) in freely moving mice. The same single unit recording and analysis, and

optostimulation parameters were used (see according sections). To obtain LFP signals, neuronal signals were bandpass filtered (0.1 Hz to 8 kHz) and digitized (32 kHz). We inspected possible seizure-like events (ictal activity) generated by optogenetic stimulations with raw traces of LFP and did not find any. Changes in brain rhythm induced by optogenetic stimulation were analyzed by plotting time-frequency spectrograms calculated using the *mtspecgramc* function in the Chronux toolbox (39).

Fear expression with optogenetic stimulation

We investigated how optically activating aIC neurons or activating specific output targets of the aIC—either to the amygdala or medial thalamus—modulates conditioned fear. On the day following conditioning, the fear expression of mice was measured with continuous optical stimulation delivered (ChR2: 473 nm, 3-8 mW; NpHR3: 593 nm, 6-8 mW; eYFP: 473 nm, 3-8 mW) during each CS presentation in context A. The fear expression paradigm for the aIC opto-stimulation was the same as the one for the single unit recording study. For the aIC terminal stimulation, bilateral optical stimulation (20 Hz pulses, 473 nm, 1-2 mW) was delivered during CS presentation in either the medial thalamus or the amygdala. Ten CSs were presented with variable inter-CS intervals (40-60 s). The behaviors of mice in each group were videotaped and scored as described above.

Tracer injection surgery

To investigate the distribution of neurons that project to either the amygdala or the medial thalamus, two retrograde tracers (CTB; Cholera toxin B) conjugated with different fluorophores were injected into a mouse. Retrograde tracers were injected into the amygdala (400 nL of 1% Alexa Fluor 488-CTB, AP: -1.2 mm, ML: -3.4 mm, DV: -4.35 mm) and the medial thalamus (400 nL of 1% Alexa Fluor 594-CTB, AP: -1.2 mm, ML: -0.2 mm, DV: -3.4

mm) in each mouse (n=3). The same surgical and injection protocols used for the viral injection in the optogenetic experiments were used.

Histology

After completion of the study, mice were overdosed with 2% avertin. To locate tetrode tips, a small electrolytic lesion was made at the tip of the recording site by passing an anodic current (10 µA, 5 s) through one tetrode channel before the perfusion. Anesthetized mice were transcardially perfused with saline (0.9%) followed by 10% buffered neutral formalin. Brains were removed and stored in 10% formalin for a day, then transferred to a 30% sucrose solution for cryoprotection. Fixed brain tissues were cut and frozen with a microtome (HM525 NX, Thermo Fisher) in coronal sections (40 µm). To locate tetrode tips, brain sections were stained with cresyl violet (Sigma, USA) and examined under a light microscope (Axioscope 5, Carl Zeiss, Germany) to locate lesions. To assess viral vector expression, sectioned brain slices were examined with a fluorescent microscope (Axioscope 5, Carl Zeiss, Germany) with a CoolLED pE 300 series illumination system. The fluorescence of retrograde tracers was imaged using a laser-scanning confocal microscope (LSM 700, Carl Zeiss, Germany).

Statistical analysis

All statistical analyses were performed using SPSS 26.0 (SPSS Inc, USA). For normally distributed samples, an unpaired two-tailed t-test or one-way ANOVA followed by Bonferroni was used to compare means between groups. A binomial proportions test was used to compare the difference between the proportions of the positive and negative groups. To compare the means of two groups with unequal variance, the Mann-Whitney U test was used. A Kruskal-Wallis test followed by Dunn’s post hoc analysis was used for comparison among

three groups with unequal variance. To compare changes that occur over time, within a group or between groups, repeated measures ANOVA followed by Bonferroni was used.

Acknowledgments

This work was supported by the National Research Foundation of Korea (NRF) grant funded by the Ministry of Science and ICT [NRF- 2021R1C1C1006607 (Y.H.), NRF-2022M3E5E8018421(J.C.), and NRF-2022R1A2C2009265(J.C.)] and by NIH grant MH099073 (J.J.K.).

Author contributions

Designed experiments: S.P., Y.H. J.J.K, and J.C. Performed experiments: S.P. and Y.H. Analyzed data: S.P. and Y.H. Supervised experiments and analysis: J.J.K, and J.C. Writing: S.P., Y.H. J.J.K, and J.C.

Declaration of interests

The authors declare that they have no competing interests.

References

1. J. J. Kim, M. W. Jung, Neural circuits and mechanisms involved in Pavlovian fear conditioning: a critical review. *Neurosci Biobehav Rev* **30**, 188-202 (2006).
2. S. Maren, M. S. Fanselow, The amygdala and fear conditioning: has the nut been cracked? *Neuron* **16**, 237-240 (1996).
3. J. L. Armony, G. J. Quirk, J. E. LeDoux, Differential effects of amygdala lesions on early and late plastic components of auditory cortex spike trains during fear conditioning. *J Neurosci* **18**, 2592-2601 (1998).
4. J. A. Gottfried, R. J. Dolan, Human orbitofrontal cortex mediates extinction learning while accessing conditioned representations of value. *Nat Neurosci* **7**, 1144-1152 (2004).
5. T. Klucken *et al.*, Neural, electrodermal and behavioral response patterns in contingency aware and unaware subjects during a picture-picture conditioning paradigm. *Neuroscience* **158**, 721-731 (2009).
6. D. C. Knight, N. S. Waters, P. A. Bandettini, Neural substrates of explicit and implicit fear memory. *Neuroimage* **45**, 208-214 (2009).
7. A. Marschner, R. Kalisch, B. Vervliet, D. Vansteenwegen, C. Buchel, Dissociable roles for the hippocampus and the amygdala in human cued versus context fear conditioning. *J Neurosci* **28**, 9030-9036 (2008).
8. J. S. Morris, R. J. Dolan, Dissociable amygdala and orbitofrontal responses during reversal fear conditioning. *Neuroimage* **22**, 372-380 (2004).
9. E. A. Phelps, M. R. Delgado, K. I. Nearing, J. E. LeDoux, Extinction learning in humans: role of the amygdala and vmPFC. *Neuron* **43**, 897-905 (2004).
10. S. E. Bruce *et al.*, Altered emotional interference processing in the amygdala and insula in women with Post-Traumatic Stress Disorder. *Neuroimage Clin* **2**, 43-49 (2012).
11. S. Yoon *et al.*, Recovery from Posttraumatic Stress Requires Dynamic and Sequential Shifts in Amygdalar Connectivities. *Neuropsychopharmacology* **42**, 454-461 (2017).
12. R. Hoehn-Saric, M. W. Schlund, S. H. Wong, Effects of citalopram on worry and brain activation in patients with generalized anxiety disorder. *Psychiatry Res* **131**, 11-21 (2004).
13. C. H. Beck, H. C. Fibiger, Conditioned fear-induced changes in behavior and in the expression of the immediate early gene c-fos: with and without diazepam pretreatment. *J Neurosci* **15**, 709-720 (1995).
14. A. K. Bruchey, F. Gonzalez-Lima, Enhanced metabolic capacity of the frontal cerebral cortex after Pavlovian conditioning. *Neuroscience* **152**, 299-307 (2008).
15. F. H. Alves *et al.*, Involvement of the insular cortex in the consolidation and expression of contextual fear conditioning. *Eur J Neurosci* **38**, 2300-2307 (2013).
16. D. H. Brunzell, J. J. Kim, Fear conditioning to tone, but not to context, is attenuated by lesions of the insular cortex and posterior extension of the intralaminar complex in rats. *Behav Neurosci* **115**, 365-375 (2001).

17. N. Gogolla, The insular cortex. *Curr Biol* **27**, R580-R586 (2017).
18. C. J. Shi, M. D. Cassell, Cortical, thalamic, and amygdaloid connections of the anterior and posterior insular cortices. *J Comp Neurol* **399**, 440-468 (1998).
19. D. A. Gehrlach *et al.*, A whole-brain connectivity map of mouse insular cortex. *Elife* **9** (2020).
20. T. Shi, S. Feng, M. Wei, W. Zhou, Role of the anterior agranular insular cortex in the modulation of fear and anxiety. *Brain Res Bull* **155**, 174-183 (2020).
21. J. P. Q. de Paiva *et al.*, The posterior insular cortex is necessary for the consolidation of tone fear conditioning. *Neurobiol Learn Mem* **179**, 107402 (2021).
22. J. P. Casanova *et al.*, A role for the interoceptive insular cortex in the consolidation of learned fear. *Behav Brain Res* **296**, 70-77 (2016).
23. S. Park, J. Cho, Y. Huh, Role of the anterior insular cortex in restraint-stress induced fear behaviors. *Sci Rep* **12**, 6504 (2022).
24. M. A. Moita, S. Rosis, Y. Zhou, J. E. LeDoux, H. T. Blair, Hippocampal place cells acquire location-specific responses to the conditioned stimulus during auditory fear conditioning. *Neuron* **37**, 485-497 (2003).
25. J. Lesting *et al.*, Patterns of coupled theta activity in amygdala-hippocampal-prefrontal cortical circuits during fear extinction. *PLoS One* **6**, e21714 (2011).
26. G. Buzsaki, Theta oscillations in the hippocampus. *Neuron* **33**, 325-340 (2002).
27. J. P. Casanova, M. Aguilar-Rivera, M. L. A. Rodriguez, T. P. Coleman, F. Torrealba, The activity of discrete sets of neurons in the posterior insula correlates with the behavioral expression and extinction of conditioned fear. *J Neurophysiol* **120**, 1906-1913 (2018).
28. O. Yizhar *et al.*, Neocortical excitation/inhibition balance in information processing and social dysfunction. *Nature* **477**, 171-178 (2011).
29. T. P. Vogels, L. F. Abbott, Gating multiple signals through detailed balance of excitation and inhibition in spiking networks. *Nat Neurosci* **12**, 483-491 (2009).
30. A. Bhatia, S. Moza, U. S. Bhalla, Precise excitation-inhibition balance controls gain and timing in the hippocampus. *Elife* **8** (2019).
31. S. Han, M. T. Soleiman, M. E. Soden, L. S. Zweifel, R. D. Palmiter, Elucidating an Affective Pain Circuit that Creates a Threat Memory. *Cell* **162**, 363-374 (2015).
32. J. P. Johansen *et al.*, Optical activation of lateral amygdala pyramidal cells instructs associative fear learning. *Proc Natl Acad Sci U S A* **107**, 12692-12697 (2010).
33. S. Lee *et al.*, Bidirectional modulation of fear extinction by mediodorsal thalamic firing in mice. *Nat Neurosci* **15**, 308-314 (2011).
34. J. Baek *et al.*, Neural circuits underlying a psychotherapeutic regimen for fear disorders. *Nature* **566**, 339-343 (2019).
35. X. Li, N. Yamawaki, J. M. Barrett, K. P. Kording, G. M. G. Shepherd, Scaling of Optogenetically Evoked Signaling in a Higher-Order Corticocortical Pathway in the Anesthetized Mouse. *Front Syst Neurosci* **12**, 16 (2018).

36. Q. Wang *et al.*, Insular cortical circuits as an executive gateway to decipher threat or extinction memory via distinct subcortical pathways. *Nat Commun* **13**, 5540 (2022).
37. N. Percie du Sert *et al.*, Reporting animal research: Explanation and elaboration for the ARRIVE guidelines 2.0. *PLoS Biol* **18**, e3000411 (2020).
38. G. Paxinos, K. B. Franklin (2008) The Mouse Brain in Stereotaxic Coordinates. Third. (Academic Press).
39. P. Mitra, *Observed brain dynamics* (Oxford University Press, 2007).

642 **Figure 1. Single unit recording of aIC neurons during conditioned fear expression.**
643 (**A**) Schematic of the auditory fear conditioning and single unit recording procedures. Neuronal
644 activities and behaviors were simultaneously recorded during the expression of conditioned fear.
645 The control group underwent the same procedures except for fear conditioning.
646 (**B**) Picture indicating the locations of aIC recording sites used for analysis. The black dots
647 represent the recording site. GI: granular insular cortex, DI: dysgranular insular cortex, AID: dorsal
648 agranular insular cortex, AIV: ventral agranular insular cortex.
649 (**C**) Sample cluster cutting of neuronal recording acquired from a tetrode.
650 (**D**) Juxtaposed action potential shape of all recorded neurons (left). Putative pyramidal neurons
651 and interneurons were distinguished based on the shape of the action potential. The plot on the
652 right shows action potential duration and repolarization. Putative pyramidal neurons are
653 represented by green dots, while putative interneurons are represented by gray dots.
654 (**E**) Freezing (fear) behavior of conditioned or control mice during five tone presentations (shaded
655 blue bars).
656 (**F**) Freezing of conditioned (left) or control (right) mice during five tone-on and tone-off sessions.
657 (**G**) Normalized (z-scored) firing rate of aIC pyramidal neurons simultaneously recorded with
658 freezing (shaded blue bars represent tone presentations).
659 (**H**) Firing rate of conditioned (left) or control (right) mice during five tone-on and tone-off
660 sessions. Paired sample t-test was used to compare means between tone-on and tone-off
661 sessions in each group (**E**-**H**). *** $P<0.001$
662 (**I**) Spectrogram of aIC local field potential recording of the conditioned and control groups before
663 and during tone presentation.
664 (**J**) Power spectrum of aIC local field potential of the conditioned and control groups.
665 (**K**) Theta power analysis before tone (left) and during tone (right) of the conditioned and control
666 groups. Cond.: conditioned group, Cont.: control group. The Mann–Whitney U test was used to
667 assess the statistical difference between the conditioned and control groups in each session. ***
668 $P<0.001$
669

670 **Figure 2. The activity of aIC pyramidal neurons bidirectionally correlates with freezing (fear)**
671 **behaviors.**
672 (**A**) Distribution of Pearson's correlation coefficient values between freezing behavior and aIC
673 neuronal activities of the fear conditioned group. The red bars represent cells with significant
674 positive correlation (positive cells), blue bars represent cells with significant negative correlation
675 (negative cells), and gray bars represent cells with no significant correlation with freezing behavior.
676 Significance was determined at $P<0.05$. Relative ratio of the non-responsive and responsive
677 (positive or negative) cell types recorded in the fear conditioned group (right pie chart).
678 (**B**) Locations of cell-types recorded. Red dot: positive/non-responsive cells, blue dot: negative or
679 non-responsive cell, red and blue gradation dot: positive/negative/non-responsive cells, gray dot:
680 non-responsive cells.

681 (**C**) Distribution of all recorded aIC neuronal activities (z-scored) before, during, and after CS (tone)
682 presentation. Each line represents the mean response of one cell to five CSs, aligned from the
683 lowest to the highest firing rate change in response to CS. The blue box represents cells classified
684 as negative cells, and the red box represents cells classified as positive cells.
685 (**D**) Example of neuronal firing for a positive cell (top right) and a negative cell (top left) over five
686 CS presentations (CS1-5). Each tick mark indicates when an action potential occurred. The peri-
687 stimulus time histogram of a positive cell (bottom right) and a negative cell (bottom left) over five
688 CS presentations.
689 (**E**) Baseline firing rate of positive cells, negative cells, non-responsive cells, and control cells. The
690 Mann-Whitney U test was used to assess statistical differences between responsive types (**
691 $P<0.01$, *** $P<0.001$).
692 (**F**) Mean (± SEM) neuronal activities of positive cells and freezing behavior. The red line
693 represents the activity of positive cells and the purple line represents freezing behavior.
694 (**G**) Mean (±SEM) neuronal activities of negative cells and freezing behavior. The blue line
695 represents the activity of negative cells and the purple line represents freezing behavior.
696 (**H**) Mean (± SEM) neuronal activities of non-responsive cells of the fear conditioned group and
697 freezing behavior. The gray line represents the activity of non-responsive cells and the purple line
698 represents freezing behavior.
699 (**I**) Absolute value of positive and negative cells firing rate changes analyzed in 1 s intervals (left).
700 The box plot shows the difference in time that each cell type takes to reach peak changes. The
701 Mann–Whitney U test was used to assess the statistical difference between the time that negative
702 and positive neurons take to reach peak firing rate change. * $P<0.05$
703 (**J**) Schematic drawing of the conditioned fear extinction procedure.
704 (**K**) Freezing (fear) behavior of mice during conditioned fear extinction (ten tone presentations,
705 N=7 mice).
706 (**L**) Distribution of Pearson's correlation coefficient values between freezing behavior and aIC
707 neuronal activities. The red bars represent cells with significant positive correlation (positive cells),
708 blue bars represent cells with significant negative correlation (negative cells), and gray bars
709 represent cells with no significant correlation with freezing behavior. Significance was determined
710 at $P<0.05$.
711 (**M**) Pearson correlation analysis for each neuronal response type and freezing behavior.
712 (**N**) Distribution of Pearson's correlation coefficient values between tone and aIC neuronal
713 activities.
714

715 **Figure 3. Optogenetic regulation of aIC pyramidal neuron output modulates conditioned fear**
716 **expression.**
717 (**A**) Schematic drawing of the experimental protocol. Experimental groups consisted of viral
718 vectors injected for excitation (AAV-CaMKII-ChR2-eYFP), inhibition (AAV-CaMKII-NpHR3-eYFP),
719 and control (AAV-CaMKII-eYFP).

720 (**B**) Histological sample showing viral expression pattern and optic fiber placement.
721 (**C**) Velocity before (baseline), during (light on), and after (light off) optostimulation of the three
722 groups in an open field test.
723 (**D**) Simultaneous single unit and local field potential (LFP) recording during the 20 Hz blue-light
724 activation of ChR2-expressing neurons. Juxtaposed unit activity (each tick indicates an action
725 potential), peri-stimulation time histogram, and LFP (left). Local brain rhythm (frequency) changes
726 induced by blue light stimulation (right).
727 (**E**) Simultaneous single unit and local field potential (LFP) recording during the continuous (cont.)
728 yellow-light activation of NpHR-expressing neurons. Juxtaposed unit activity (each tick indicates
729 an action potential), peri-stimulation time histogram, and LFP (left). Local brain rhythm (frequency)
730 changes induced by yellow light stimulation (right).
731 (**F**) Mean (± SEM) freezing behavior of mice during the five CS (tone) and optostimulation delivery.
732 (**G**) Freezing behavior of the five tone-on with optostimulation and tone-off periods
733 (Kruskal–Wallis test; **P<0.01, ***P<0.001).
734 (**H**) Comparison between the first and the last tone+optostimulation and tone-off session freezing
735 behavior among groups (Wilcoxon signed ranks test; **P<0.01).
736 (**I**) Mean (± SEM) freezing behavior of mice during five CS-only presentations without any
737 optostimulation.
738 (**J**) Freezing behavior of the five tone-on and tone-off periods.
739 (**K**) Comparison between the first and the last tone and tone-off session freezing behavior among
740 groups.
741 (**F**-**K**) Blue line represents optical excitation (ChR2, n=13), yellow line represents optical inhibition
742 (NpHR3, n=7), and gray line represents control (eYFP, n=13).
743 (**F**, **G**, **L**, **J**) The Kruskal–Wallis test was used to test statistical significance of among groups
744 (**H** and **K**) The Wilcoxon signed ranks test was used to compare means of freezing behavior
745 between first and last sessions in each group.
746

747 **Figure 4. Tracing of aIC neurons that projects to the thalamus or the amygdala.**
748 (**A**) Schematic drawing of cholera toxin B (CTB) retrograde tracers injected into the amygdala
749 (green) and thalamus (red).
750 (**B**) Image showing the injection sites.
751 (**C**) High-resolution of the panel b image. sm: stria medullaris of the thalamus, LHb: lateral
752 habenular nucleus, MHb: medial habenular nucleus, DG: dentate gyrus, PV: paraventricular
753 thalamic nucleus, IMD: intermediodorsal thalamic nucleus, MDM: mediodorsal thalamic nucleus,
754 medial part, MDC: mediodorsal thalamic nucleus, central part, MDL: mediodorsal thalamic nucleus,
755 lateral part, CM: central medial thalamic nucleus, LaDL: lateral amygdaloid nucleus, dorsolateral
756 part, and BLA: basolateral amygdaloid nucleus, anterior part.
757 (**D**) Sample image of neurons in the aIC that either project to the thalamus (red) or the amygdala
758 (green). A high-resolution image of the thalamus-projecting aIC neurons is shown on the left, and

759 that of the amygdala-projecting aIC neurons is shown on the right. M2: secondary motor cortex,
760 M1: primary motor cortex, S1: primary somatosensory cortex, GI: granular insular cortex, DI:
761 dysgranular insular cortex, AID: agranular insular cortex, dorsal part, AIV: agranular insular cortex,
762 ventral part, Pir: piriform cortex, Den: dorsal endopiriform nucleus, CPu: caudate putamen
763 (striatum), and AcbC: accumbens nucleus, core.
764 (**E**) The number of aIC neurons that were labeled to either project to the thalamus (Alexa fluor
765 594, n=3 mice) or the amygdala (Alexa fluor 488, n=3 mice). Data are presented as mean ± SEM.
766 The Mann-Whitney U test was used to assess statistical difference (* $P<0.05$).
767

768 **Figure 5. Specific optogenetic activation of aIC projection to the medial thalamus or the**
769 **amygdala bidirectionally regulate conditioned fear expression.**
770 (**A**) Schematic drawing of the adeno-associated virus (AAV) injection and optostimulation sites.
771 Viral vectors for opsin expression (AAV-CaMKII-ChR2-eYFP) or control (AAV-CaMKII-eYFP) were
772 bilaterally injected in the aIC, and bilateral optostimulation was delivered in the mid-thalamic
773 region.
774 (**B**) Example expression pattern of aIC projection terminals in the thalamic region and the location
775 of bilateral optic fiber placement outlined by dashed lines. LHb: lateral habenular nucleus, MHb:
776 medial habenular nucleus, PV: paraventricular thalamic nucleus, IMD: intermediodorsal thalamic
777 nucleus, MDM: mediodorsal thalamic nucleus, medial part, MDC: mediodorsal thalamic
778 nucleus, central part, MDL: mediodorsal thalamic nucleus, lateral part, CM: central medial thalamic
779 nucleus.
780 (**C**) Mean (±SEM) freezing behavior of mice expressing ChR2 (n=12) or control (eYFP, n=8)
781 induced by optostimulation of aIC projection terminating in the thalamus to repeated CS (tone).
782 Blue bars indicate when tone and optostimulation were delivered. Last point indicates freezing
783 behavior when tone was delivered without optostimulation 24h after the extinction protocol
784 (retrieval).
785 (**D**) Freezing behavior during the "Tone on+optostim" and "Tone off" of the aIC thalamus ChR2
786 and control groups.
787 (**E**) Schematic drawing of AAV injection and optostimulation sites. Viral vectors for opsin
788 expression (AAV-CaMKII-ChR2-eYFP) or control (AAV-CaMKII-eYFP) were bilaterally injected in the
789 aIC, and bilateral optostimulation was delivered in the anterior-amygdala region.
790 (**F**) Example expression pattern of aIC projection terminals in the amygdala and location of
791 bilateral optic fiber placement outlined by dashed lines. CeA: central nucleus of the amygdala, BLA:
792 basolateral amygdaloid nucleus, anterior part.
793 (**G**) Mean (± SEM) freezing behaviors of mice expressing ChR2 (n=6) or control (eYFP, n=6)
794 induced by optostimulation of aIC projection terminating in the amygdala to repeated CS (tone).
795 Blue bars indicate when tone and optostimulation were delivered. Last point indicates freezing
796 behavior when tone was delivered without optostimulation 24h after the extinction protocol
797 (retrieval).

(**H**) Freezing behavior during the "Tone on+optostim" and "Tone off" of the aIC-amygdala ChR2 and control groups.

(**C** and **G**) Two-way repeated measure ANOVAs were performed to compare freezing behavior between groups (C and G).

(**D** and **H**) Paired t-test was used to compare means of "Tone on+optostim" and "Tone off" in each group. (*P<0.05, **P<0.01, ***P<0.001).

Behavioral paradigm

Neural recording in aIC

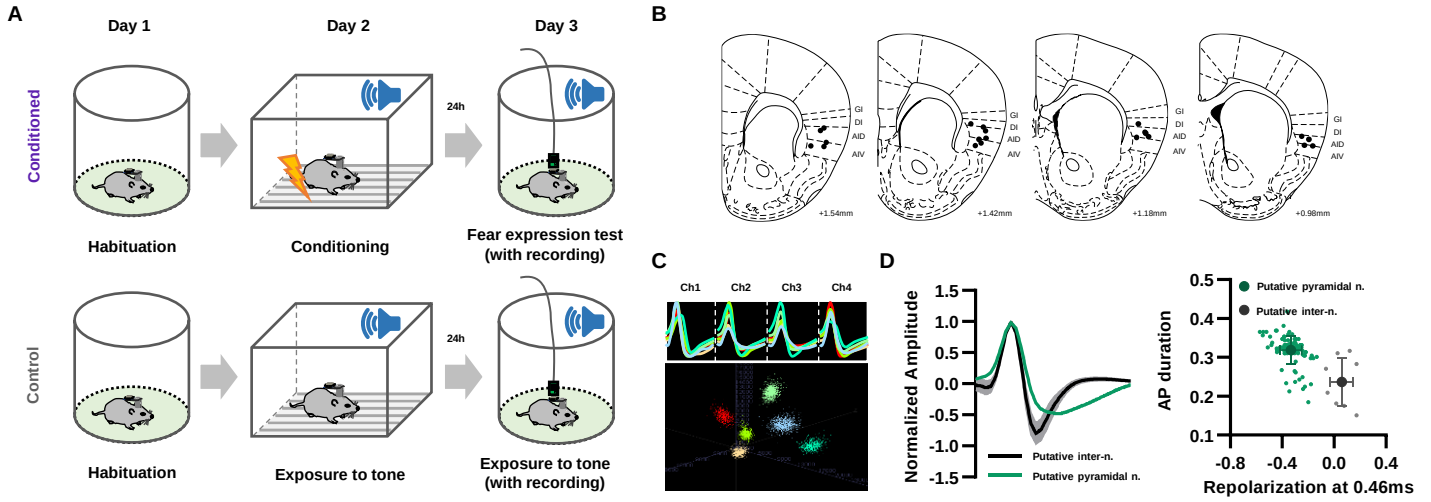

Expression of conditioned fear & Associated aIC neural signal

Analysis of aIC local field potential

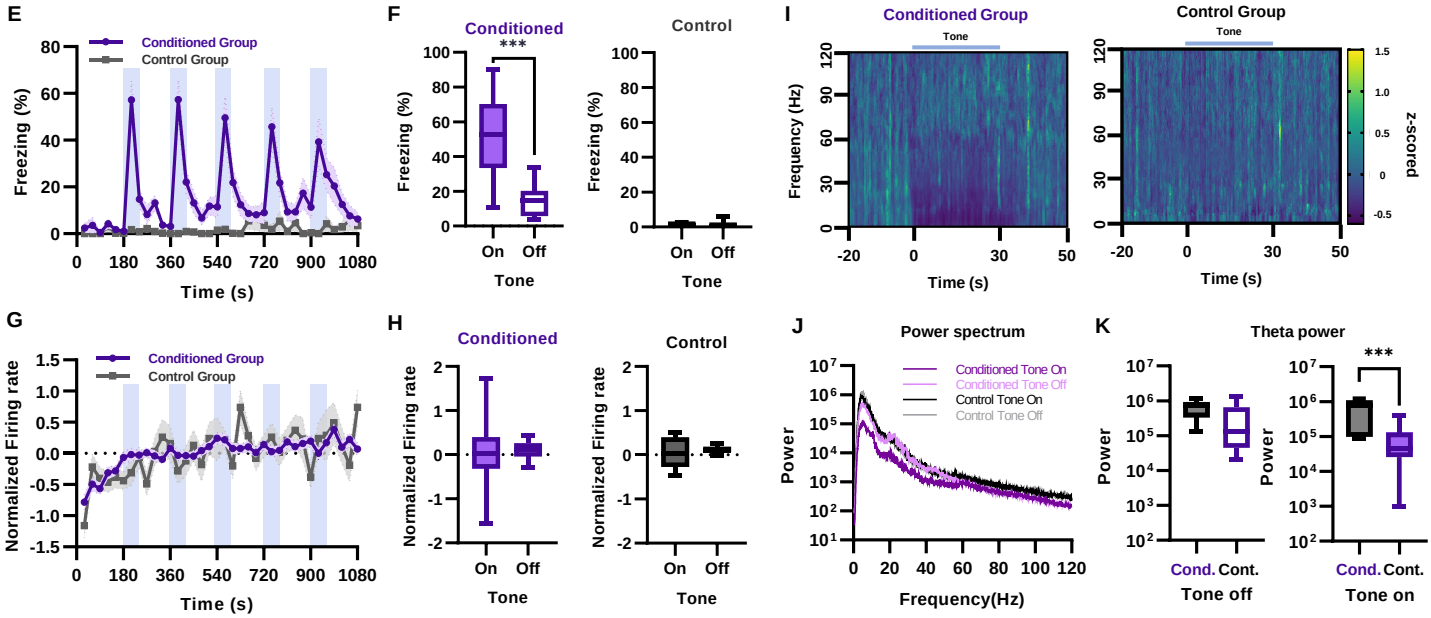

Response types of aIC neurons

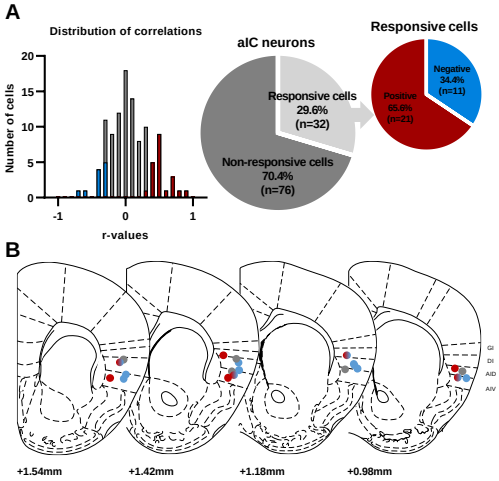

Distribution of aIC response types

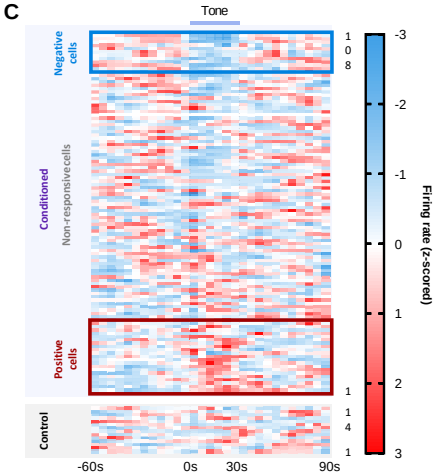

Basic properties of aIC response types

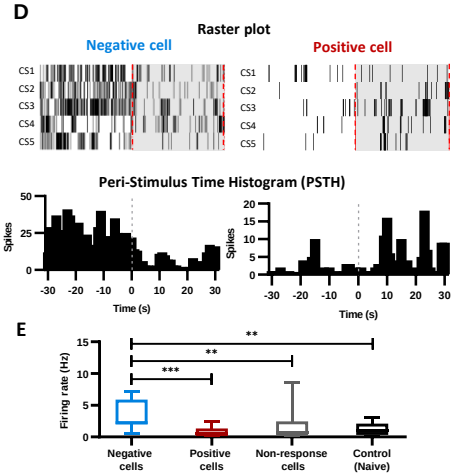

Firing rate of aIC response types and freezing behavior

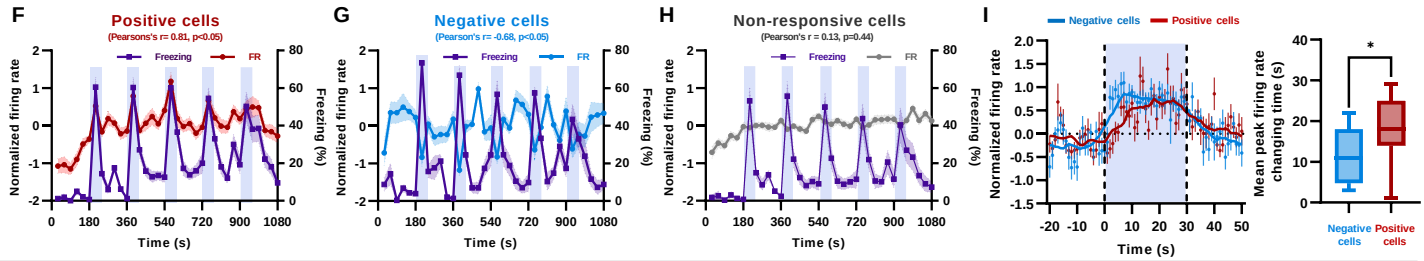

Firing rate of aIC response types and freezing behavior during extinction

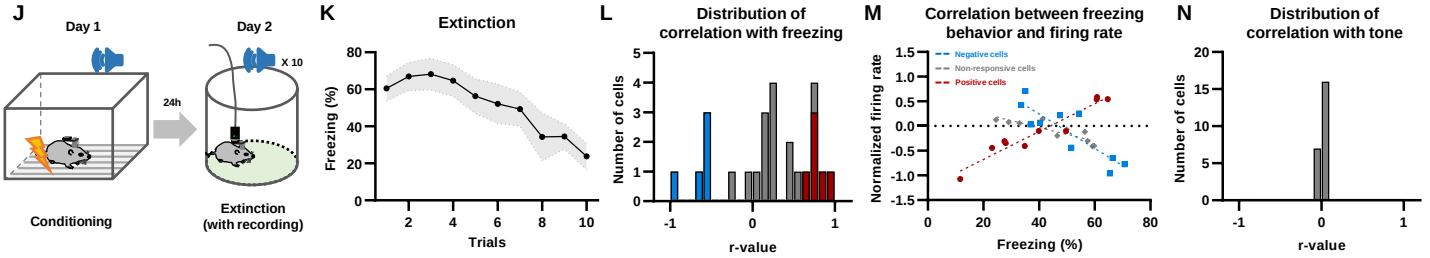

aIC optogenetic experiment

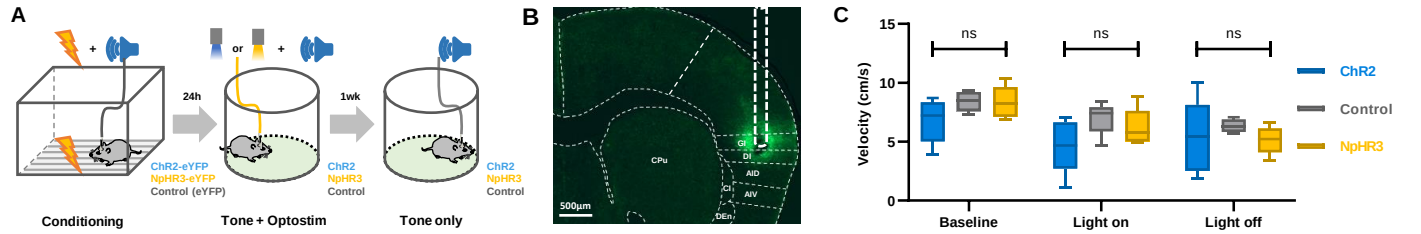

aIC neuronal activity changes induced by optostimulation

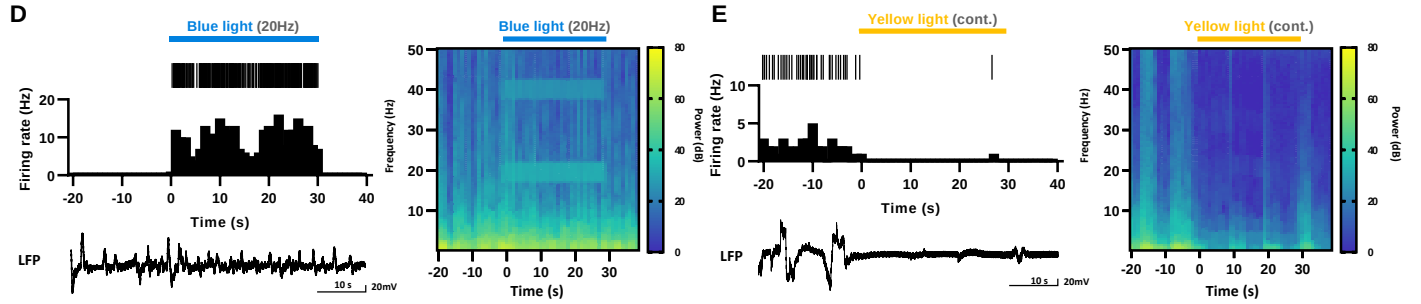

Optogenetic aIC stimulation and conditioned fear

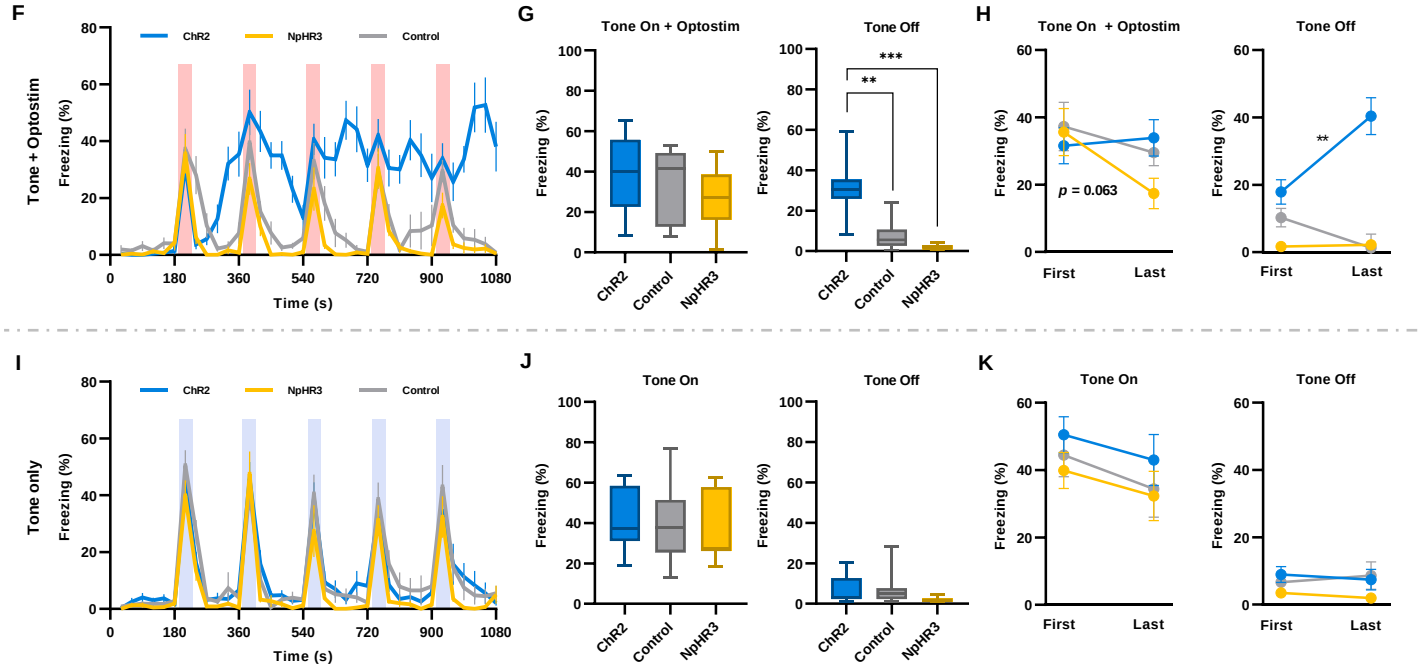

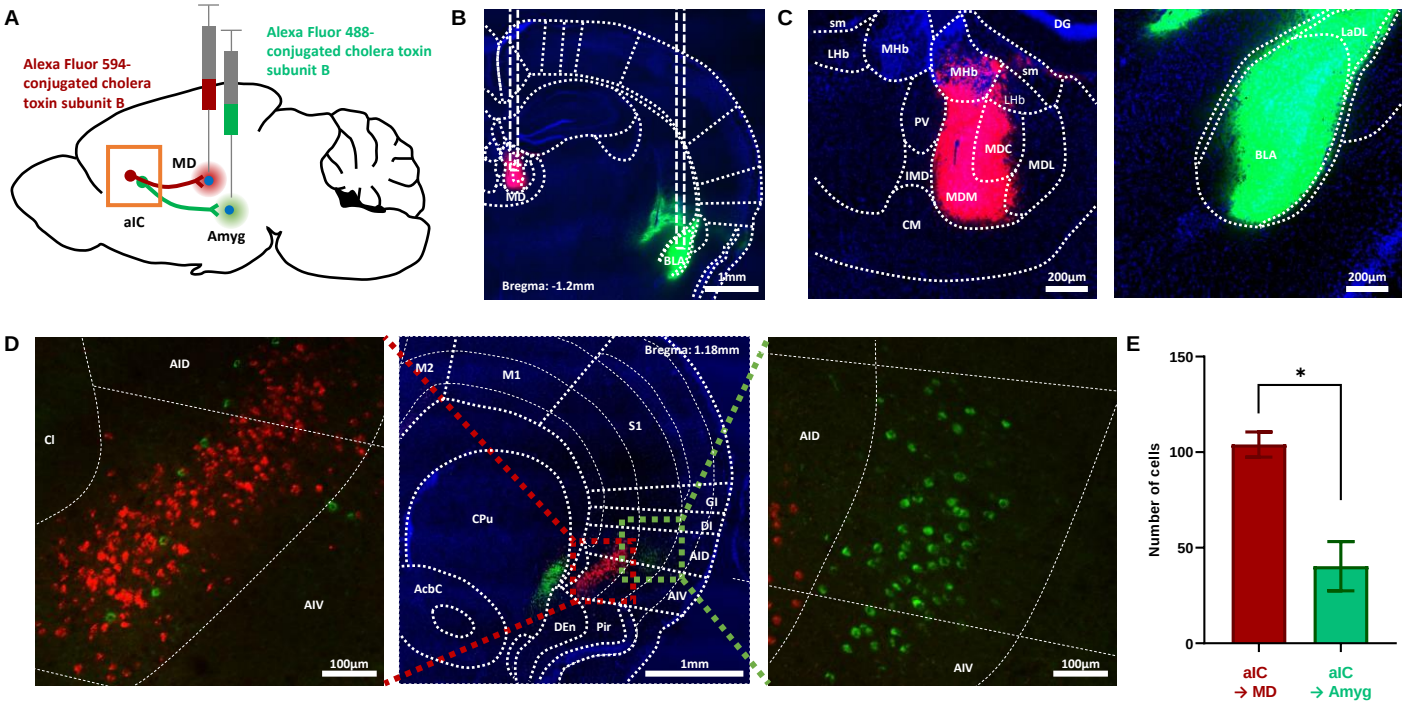
A
Alexa Fluor 594-conjugated cholera toxin subunit B
Alexa Fluor 488-conjugated cholera toxin subunit B
MD
aIC
Amyg
B
MD
BLA
Bregma: -1.2mm
1mm
C
sm
DG
LHb
MHb
MHb
sm
LHb
PV
MDC
MDL
IMD
MDM
CM
200µm
LaDL
BLA
200µm
D
AID
CI
AIV
100µm
Bregma: 1.18mm
M2
M1
S1
CPu
GI
DI
AID
AcbC
AIV
DEn
Pir
1mm
AID
AIV
100µm
E
Number of cells
150
100
50
0
*
aIC → MD
aIC → Amyg

aIC → Medial Thalamus optogenetics

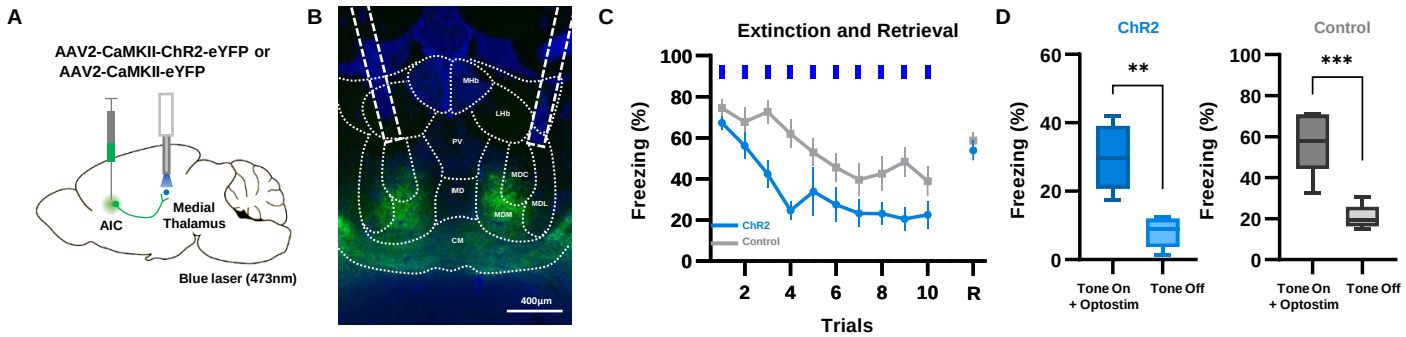
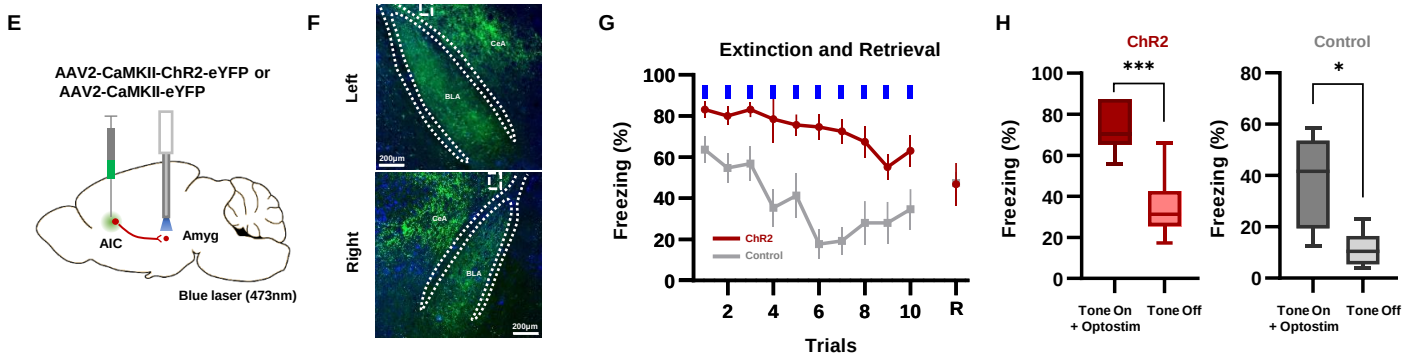
aIC → Amygdala optogenetics